

# Using Whispering Gallery Mode Resonators to Accurately Track Temperature Fluctuations

Bain Alexander Bronner

*Adviser: Dr. Eugeny Mikhailov*

## **Abstract**

Whispering Gallery Mode Resonators (WGMRs) are optical resonant cavities. By producing high Q-factor disks, the aim is to create miniature sensors which are able to track environmental variables (such as temperature) with high precision. Fabrication of the disks and coupling into the resonators is outlined and studied as well. A  $Q > 10^8$  has been produced in this study, as well as coupling of over 60%. We were able to resolve temperature shifts down to about 500  $nK$ , limited by electronic noise. Future outlooks are also mentioned.

# Contents

1	Introduction	3
2	Theory	4
3	Resonator Fabrication and Coupling	6
4	Results	12
5	Temperature Tracking	15
6	Conclusions and Outlooks	17
7	Acknowledgments	18
	Appendices	20
A	Polishing Technique	20
B	Coupling Plots	23

# List of Figures

3.1	Assorted WGMRs . . . . .	7
3.2	A block diagram of the experimental setup . . . . .	8
3.3	Diamond prism with ruler in background. The largest tick mark corresponds to one centimeter . . . . .	9
3.4	Coupling diagram generated with our code: $\phi = 34.57^\circ$ . . . . .	10
3.5	Beam trace generated with our code; the opacity of the beam indicates relative intensity, while the two colors represent different polarizations of light. . . . .	10
3.6	Two coupling set-ups (beams added for visual aid) . . . . .	11
3.7	Resonant Mode Contrast . . . . .	13
4.1	Whispering Gallery Modes with $^{87}\text{Rb}$ Spectra . . . . .	13
4.2	Newton's rings produced by a WGMR disk . . . . .	14
4.3	Comparing modes (a) and (b), the difference in width can be seen. It was about a factor of three. . . . .	15
5.1	Temperature sensitivity using resonant mode frequency . . . . .	16
5.2	The response signal along with the mode being tracked. The noise in the mode is due to dithering the laser . . . . .	18
B.1	Coupling Angles for Diamond Prism, Lithium Niobate Disk . . . . .	23
B.2	Beam Trace for Diamond Prism, Lithium Niobate Disk . . . . .	23



# 1 Introduction

The main purpose of this experiment was to realize precise measurements of temperature change, by tracking an optical resonant cavity. The optical cavities used were Whispering Gallery Mode Resonators (WGMRs), which can store light for long periods of time, with little loss [1]. The main interest was to keep track of the resonant frequency for a given mode, and whilst knowing the thermal expansion coefficient and the change in the index of refraction with temperature [2], the change in resonant frequency could be converted to a change in temperature of the resonator volume.

The traditional Fabry-Perot (FP) resonator, while useful in many applications, is not well suited for this kind of measurement. High quality FP resonators tend to be expensive, complex, and prone to vibration instabilities due to low-frequency mechanical resonances. For this application, the stability and relatively small size of the resonator are very important [3]. The response time is directly related to the heat capacity of the resonator, thus smaller resonators will have a faster response. Further, any instabilities in the resonator would degrade measurement capabilities.

Whispering gallery mode resonators lend themselves well to this kind of measurement. Unlike Fabry-Perot resonators, no mirrors are used to contain the electromagnetic wave. Instead, it is confined to the resonator by total internal reflection. As a result, no large separation nor ultra-high quality mirrors need to be used. These resonators can be fabricated with a very high Quality Factor (Q-factor, defined in Equations (2.1) and (2.2)), yet be very small in size, usually on the micrometer to millimeter scale.

High Q-factors imply narrow resonant widths as well as longer lifetimes for the resonating wave. Thus optical path lengths of hundreds or thousands of meters are created. Q-factors of  $10^{11}$  have been reported [4], while Q's in excess of  $10^8$  have been produced in our lab. Further, the small size of WGMRs allow them to respond fairly quickly to changes in the environment. Therefore, they were chosen for this measurement/experiment.

## 2 Theory

Q-factor and finesse are the two most important quantities when discussing resonators. Beginning with Q-factor, it is defined as follows:

$$Q \sim \frac{\text{Energy Stored}}{\text{Energy Dissipated per Cycle}}, \quad (2.1)$$

however, to actually measure it for a given resonator, it can be defined as:

$$Q = \frac{\nu_0}{\Delta\nu} = \nu_0 T_{rt} \frac{2\pi}{l}, \quad (2.2)$$

which is valid in the high Q regime. In Equation (2.2),  $\nu_0$  is the frequency of the light and  $\Delta\nu$  is the resonant mode's full-width at half-maximum.  $T_{rt}$  is the round-trip time i.e. one trip around the circumference of the disk, and  $l$  is the round-trip loss. From that equation, one can see that narrower mode widths correspond with higher Q-factors, as well as diminishing losses.

Finesse, on the other hand, is a measure of the free spectral range (FSR) divided by the mode width. The FSR of a given resonator is defined as:

$$\text{FSR} = \frac{c}{2n_{\text{eff}}\pi R}, \quad (2.3)$$

where  $c$  is the speed of light,  $n_{\text{eff}}$  is the effective index of refraction of the resonator, and  $R$  is the radius of the disk [5]. As can be seen in Equation (2.3), smaller disks have a larger free spectral range. Finesse is related to the Q-factor by:

$$\mathcal{F} = \frac{\lambda Q}{n_{\text{eff}} L_{\text{cav}}}, \quad (2.4)$$

where  $n_{\text{eff}}$  is the effective index of refraction and  $L_{\text{cav}}$  is the path length. For disk resonators,  $L_{\text{cav}} = 2\pi R$ , where  $R$  is the radius of the disk. From this point, the focus will be on the more easily measured quantity, the Q-factor.

To measure temperature changes, we track the resonant modes' position, given by this formula:

$$\nu = m \frac{c}{2\pi R(T)n(T)}, \quad (2.5)$$

where the radius of the disk ( $R$ ) and the index of refraction ( $n$ ) are both temperature dependent, and  $m$  is the mode number. Thus, the resonant frequency is a function of temperature, and we can calculate changes in  $T$ , by measuring the shift in it, using:

$$\Delta T = \frac{-\Delta\nu}{\nu_0 \left( n \frac{\partial n}{\partial T} + \alpha \right)}, \quad (2.6)$$

where  $\partial n / \partial T$  is the change in the index of refraction with respect to temperature,  $\alpha$  is the thermal expansion coefficient, and  $\nu_0$  is the unperturbed resonant frequency. Rearranging Equation (2.6), the change in frequency per degree Celsius is:

$$\frac{\Delta\nu}{\Delta T} = -\nu_0 \left( n \frac{\partial n}{\partial T} + \alpha \right) = \gamma, \quad (2.7)$$

where  $\gamma$  is used to denote the proportionality constant. The accuracy of the temperature measurement is related to the accuracy of the measured resonance shift ( $\Delta\nu$ ). Since Q-factor and mode width are inversely related, and changes in temperature are directly proportional to mode frequency shift, higher Q-factors are desirable for greater precision in resolving small temperature changes. This can be readily seen with the following thought experiment: if a given mode is 300 MHz wide, then a shift of 3 MHz is only 1% of the total width. However, a mode that is 3 MHz wide would shift by its entire line-width. Thus, for a given change in temperature, narrower modes are desired.

Increasing Q-factors also correspond with longer optical interaction lengths. By replacing  $\nu_0$  in Equation (2.2) with  $c/\lambda$ , and rearranging, one arrives at a formula for the average distance a given photon will travel inside of the resonator. Namely:

$$d = Q\lambda, \tag{2.8}$$

where  $\lambda$  is the wavelength of the resonant light. Longer photon travel distances allow smaller changes in the resonator to be more noticeable, since these small changes are experienced each round trip. This leads to an ability to track smaller variations in temperature. Further, by utilizing a laser-lock, shifts in resonant frequency can be measured to fractions of the mode width.

### 3 Resonator Fabrication and Coupling

Calcium fluoride ( $\text{CaF}_2$ ) and lithium niobate ( $\text{LiNbO}_3$ ) WGMR disks have been produced. The disks were created by drilling circular blanks out of a crystalline window, and then mounting them onto brass posts. Subsequent rounds of shaping and polishing were done on a lathe using progressively finer lapping paper, while cleaning the disks with acetone between steps. The final two steps involved using a  $0.5 \mu\text{m}$  and  $0.1 \mu\text{m}$  diamond emulsion fluid [see Appendix A]. An example of polished and shaped disks we've used is in Figure 3.1. Using this procedure, a Q-factor greater than  $10^8$  has been measured with a  $\text{LiNbO}_3$  disk.

The next step is coupling, or actually getting light into the resonator. A simplified block diagram of the experimental setup is in Figure 3.2. Whispering gallery mode resonators can be coupled into by a few different methods. In this case, prism coupling was employed, using both a  $45^\circ$  rutile ( $\text{TiO}_2$ ) and  $60^\circ$  diamond prism at different points. The diamond prism is shown in Figure 3.3. As can be seen in the picture, the prism faces are less than two millimeters wide.

Prism coupling is based on a few principles. The first is the evanescent wave. At the point of total internal reflection, an exponentially decaying wave exists outside of the prism-air interface. This follows from one of Maxwell Equations' boundary conditions that the electric field must be continuous at the interface [7]. By placing the disk in this region, frustrated



(a) A Calcium Fluoride WGMR, 7mm in diameter ( $Q \simeq 1 \times 10^7$ )



(b) A Lithium Niobate WGMR, 7mm in diameter ( $Q \simeq 1.5 \times 10^8$ )

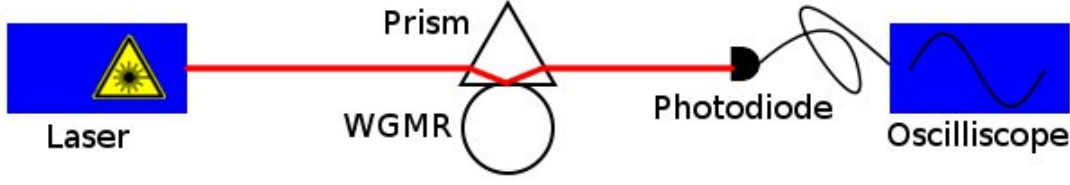


(c) A Potassium Lithium Niobate WGMR, 0.66mm in diameter (Polished by JPL,  $Q \sim 10^7$ )



(d) A Lithium Niobate WGMR, 1.6mm in diameter (Polished by JPL,  $Q \simeq 5 \times 10^7$ )

Figure 3.1: Assorted WGMRs



## Simplified Experimental Set-up

Figure 3.2: A block diagram of the experimental setup

total internal reflection can take place, which is analogous to quantum mechanical tunneling. Thus, power can be transmitted from the prism to the resonator.

In addition, the input beam needs to be focused inside the prism at an angle that provides phase matching between the evanescent wave of the total internal reflection spot and the WGMR, respectively. The angle that meets this requirement satisfies the following:

$$\sin \phi \simeq \frac{n_r}{n_p}, \quad (3.1)$$

where  $\phi$  is the critical angle,  $n_r$  is the index of refraction of the disk resonator, and  $n_p$  is the index of refraction of the prism [6]. See Figures 3.4 and 3.5 for an illustration, and Figure 3.6 for a picture of two actual disk/prism combinations. Appendix B contains similar plots for other disk/prism combinations used in this study.

Another criteria for coupling is the beam shape. It must be adjusted to maximize the overlap of the internal resonating and incoming modes. In other words, the beam needs to be related to the shape of the resonator-prism contact point. This is called aperture matching and is achieved when the same critical angle  $\phi$  in Equation (3.1) also satisfies:

$$\cos \phi \simeq \sqrt{\frac{r}{R}}, \quad (3.2)$$

where  $r$  is the vertical radius of curvature and  $R$  is the horizontal radius of curvature of the resonator, both near the contact spot. By combining Equations (3.1) and (3.2), an equation

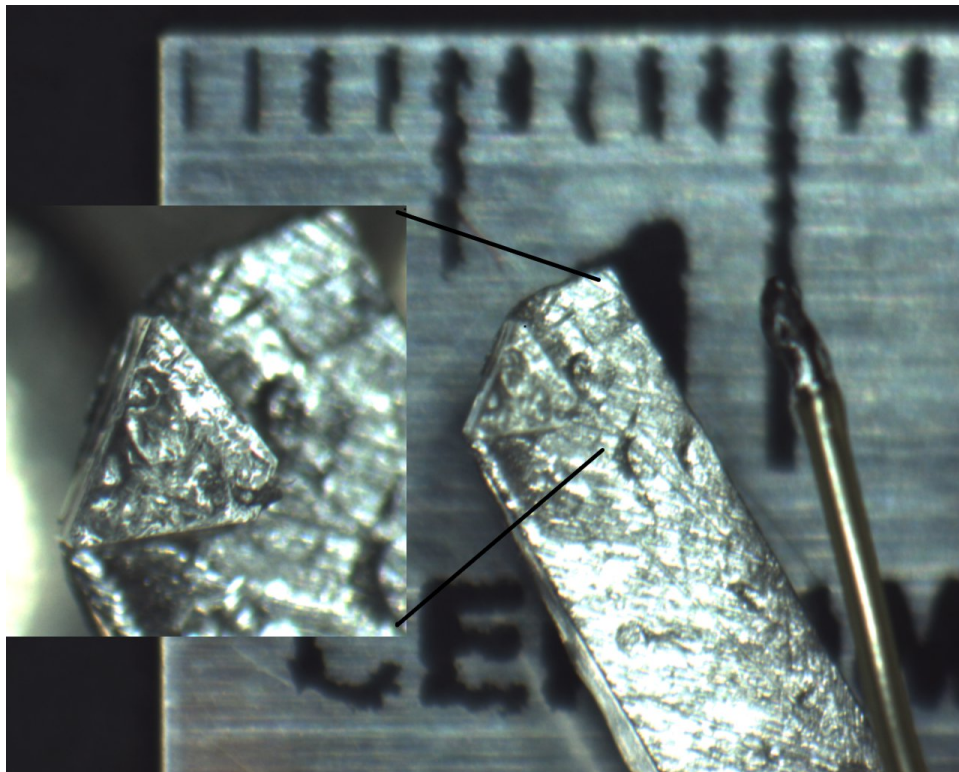


Figure 3.3: Diamond prism with ruler in background. The largest tick mark corresponds to one centimeter

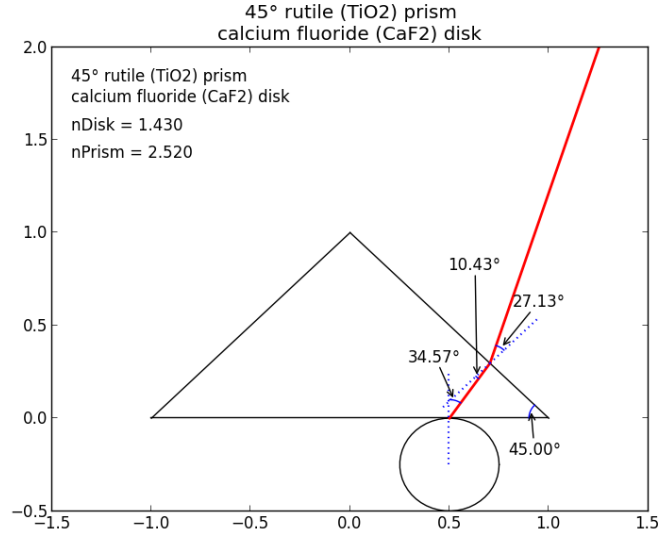


Figure 3.4: Coupling diagram generated with our code:  $\phi = 34.57^\circ$

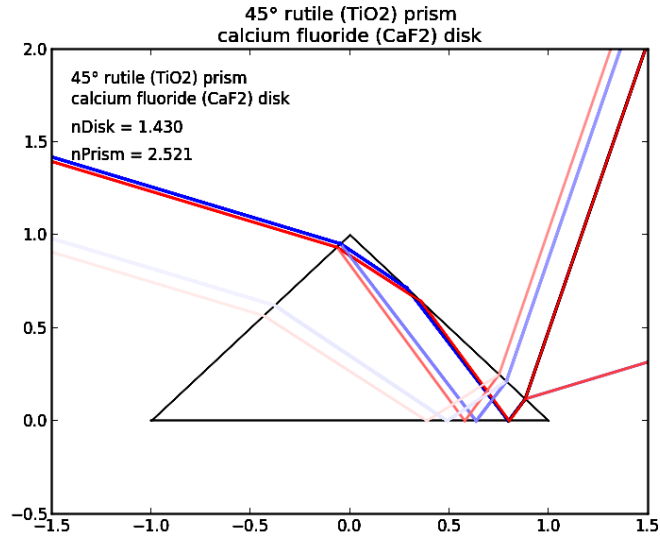


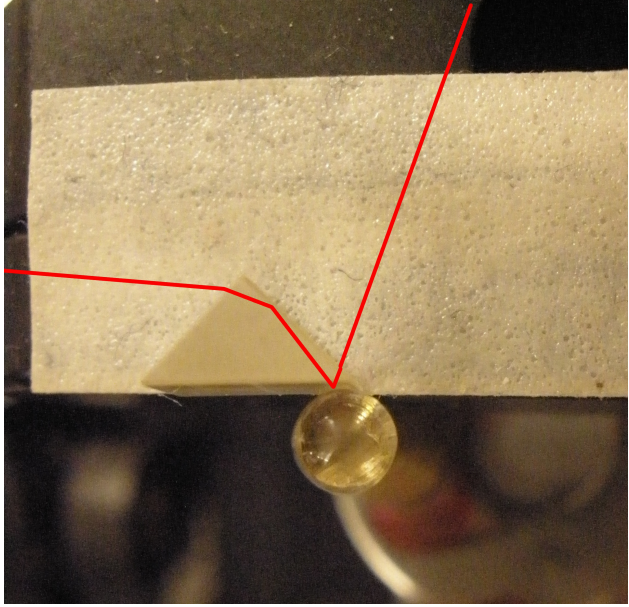
Figure 3.5: Beam trace generated with our code; the opacity of the beam indicates relative intensity, while the two colors represent different polarizations of light.

for the ideal vertical radius of curvature is obtained. Namely:

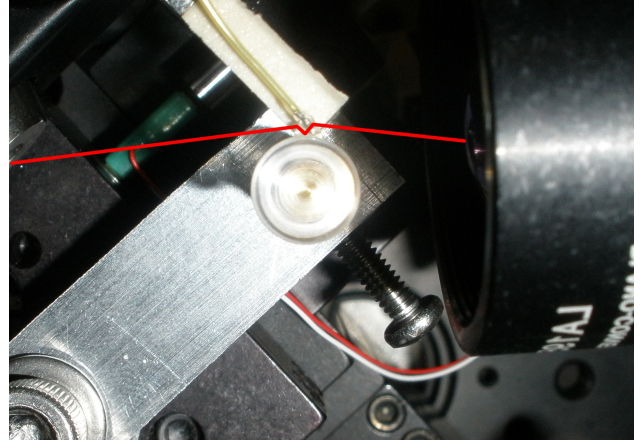
$$r = R \left[ 1 - \left( \frac{n_r}{n_p} \right)^2 \right]. \quad (3.3)$$

Lastly, the distance between the resonator and prism must be adjusted to meet the critical





(a) Coupling picture with rutile prism and  $\text{CaF}_2$  disk



(b) Coupling picture with diamond prism and  $\text{LiNbO}_3$  disk

Figure 3.6: Two coupling set-ups (beams added for visual aid)

coupling conditions, which is when the largest amount of power is transferred from the pump beam into the resonator. To accomplish this, the power transferred must exactly match any intrinsic losses [6]. The adjustment of this distance alters the strength of the input field, since the evanescent field exponentially decays with distance from the prism. When the input field provides more power than is lost in the resonator, it is said to be “over-coupled;” when the internal losses are greater than the incoming field, it is said to be “under-coupled.”

The coupling level is described by the mode absorption relative to the mean voltage of the transmission signal. Figure 3.7 shows a coupling contrast level from this experiment. The general procedure used to achieve coupling follows:

- To initially get the beam spot focused on the disk, the angle was set to slightly less than the critical angle. That is, it was set so that the beam would not totally-internally-reflect, but rather refract into the resonator. Once the disk-prism contact spot was found by observing illumination of the disk, the angle was adjusted to the critical point.
- The best horizontal angle was usually slightly different from the theoretical predictions.

The best angle was found by searching around the predicted one. Q-factor would not increase or decrease during this time, rather the coupling level would go up and down. Once this angle was optimized, attention turned to the vertical angle of the prism.

- The vertical angle of the coupling prism played a large role in the coupling level; very small changes had drastic effects. By adjusting this angle in small amounts, the angle of the probe beam was adjusted to be parallel with the disk-rim plane. Once again, coupling contrast was optimized.
- The focal length of the lens (and the subsequent beam waist size) used also made a significant difference in coupling. After time, the most effective technique for determining the appropriate lens became viewing the transmission beam on a sheet of paper, through an infrared viewer. As the resonator was brought into coupling, the size of the beam spot compared to the contact spot size could be observed. If the contact spot was smaller than the beam, a shorter focal length was employed; if the opposite was observed, a larger focal length was used.
- Using these techniques, a mode-contrast of almost 70% has been observed.

## 4 Results

Initially, research was focused on increasing the Q-factor to allow for precise measurements. After much trial and error, a procedure was developed which allowed for the creation of a WGMR disk with  $Q > 10^8$ . The full procedure is listed in Appendix A. An example of the resonant modes is in Figure 4.1.

During the same time as Q-factor experiments, various measurements were taken of the disk rim. The horizontal radius of curvature is easily measured using a microscope, however measuring the vertical radius of curvature is difficult using the same technique, since the vertical radius is not continued for the whole disk; it is a curvature localized to the rim.

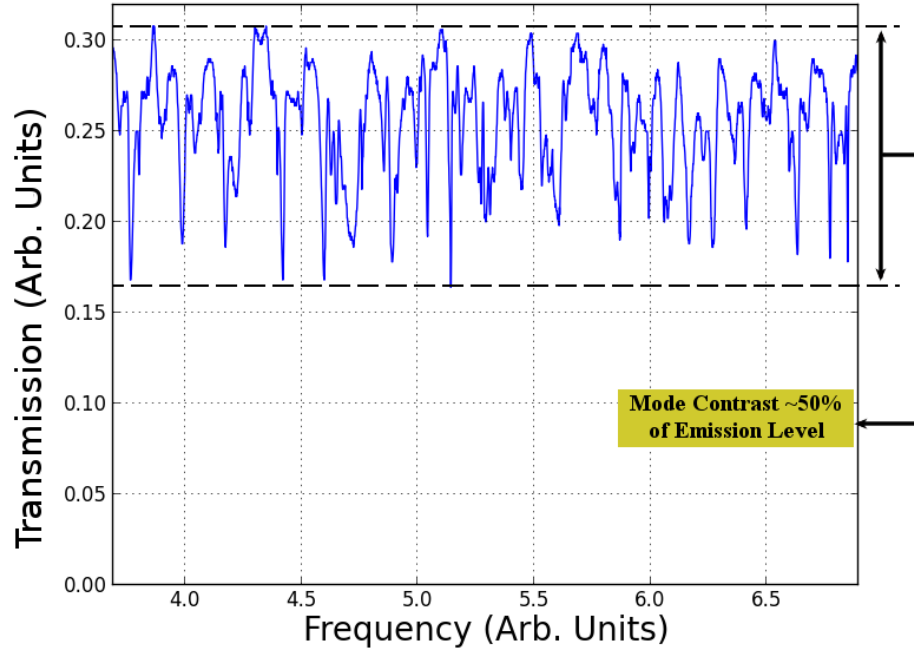


Figure 3.7: Resonant Mode Contrast

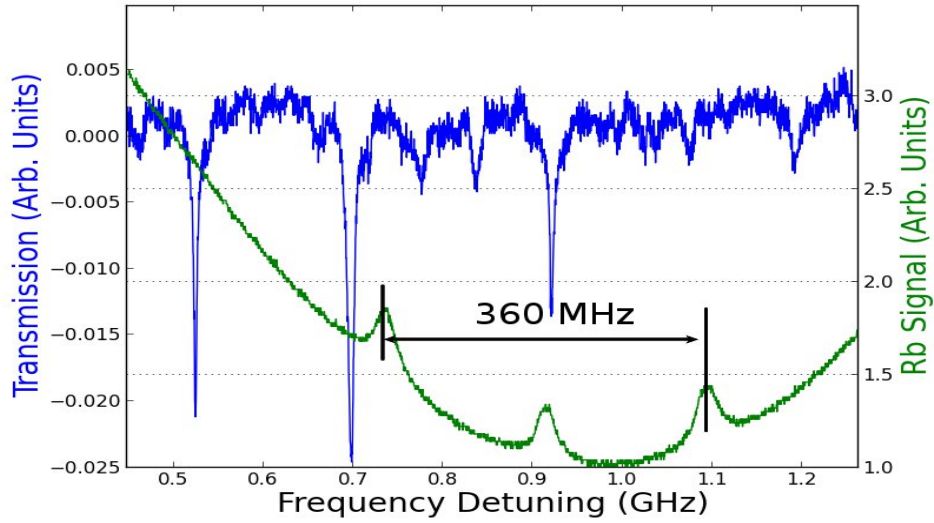


Figure 4.1: Whispering Gallery Modes with  $^{87}\text{Rb}$  Spectra

Alternatively, in order to get an accurate idea of the shape of the disk, Newton rings were observed reflecting off of the contact point. By making the probe beam significantly larger than the contact spot, rim shape could be deduced. The resulting Newton rings were able

to depict both the vertical and horizontal radius through the following relation:

$$r_N = \left[ \left( N - \frac{1}{2} \right) \lambda R \right]^{1/2}, \quad (4.1)$$

where  $N$  is the bright ring number,  $\lambda$  is the wavelength of light, and  $R$  is the radius of curvature. One of these pictures is in Figure 4.2. In order to estimate the curvature, the optical elements between the disk and camera need to be taken into account.

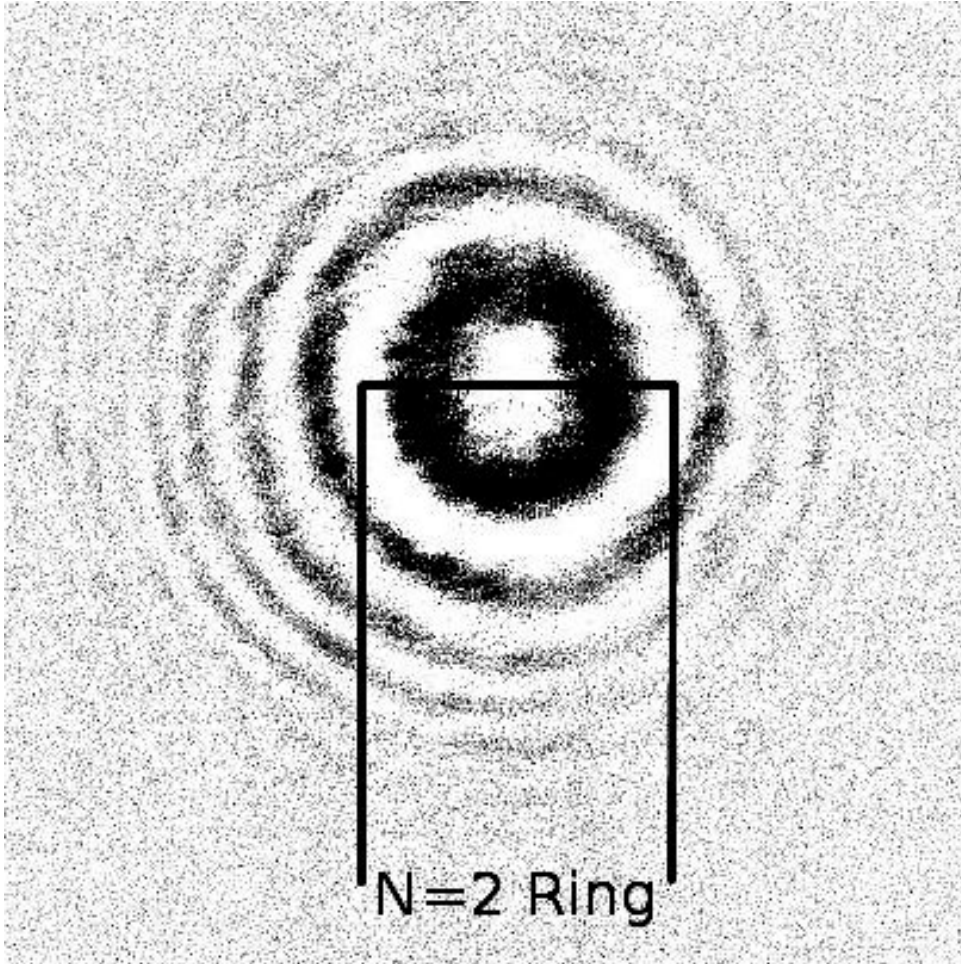
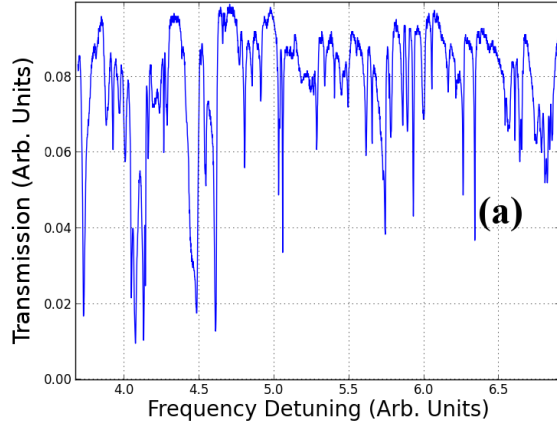
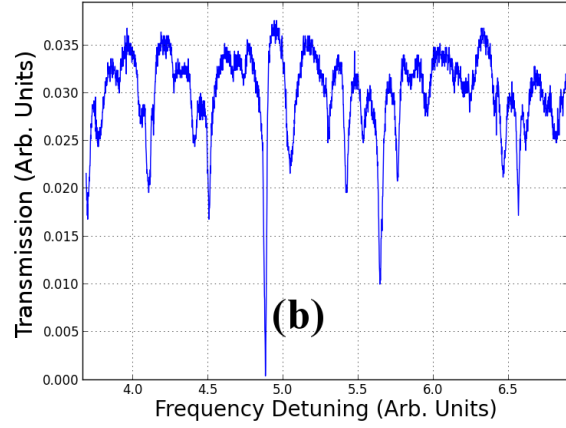


Figure 4.2: Newton's rings produced by a WGMR disk

Another venture into the properties of WGMRs was done by changing the polarization of the probe beam. It was found that polarization in the plane of the disk produced narrower modes than vertical polarization. The difference was about a factor of three, which can be seen in Figure 4.3. To rule out time-degradation of the disk, these measurements were



(a) Horizontal Polarization (plane of the disk)



(b) Vertical Polarization

Figure 4.3: Comparing modes (a) and (b), the difference in width can be seen. It was about a factor of three.

conducted within 30 minutes of one another.

## 5 Temperature Tracking

After those initial tests, temperature tracking was done visually on an oscilloscope, using a thermistor as a reference. This was done for both  $\text{CaF}_2$  and  $\text{LiNbO}_3$ . Using reported values for  $\partial n / \partial T$  and  $\alpha$  [8], an expected response of  $4.21 \text{ GHz/K}$  was calculated for  $\text{CaF}_2$ . The measured shifts in resonant position were:  $4.13$ ,  $4.10$ , and  $3.91 \text{ GHz/K}$ . The average for these measurements was  $4.05 \text{ GHz/K}$ , which was in good agreement with the expected value. A similar test was done with  $\text{LiNbO}_3$ . A plot containing the temperature change measured by a thermistor and the resonance position is in Figure 5.1.

After testing of the concept and demonstrating that it followed the theory, a lock-in amplifier was employed to electronically track mode position. By measuring the feedback signal, the relative mode shift can be calculated, and then converted into a temperature change. To calculate the smallest voltage change that could be attributed to temperature shift, the noise level of the signal had to be taken into account. The signal-to-noise ratio provides the level to which one could resolve any changes. The following formula provides



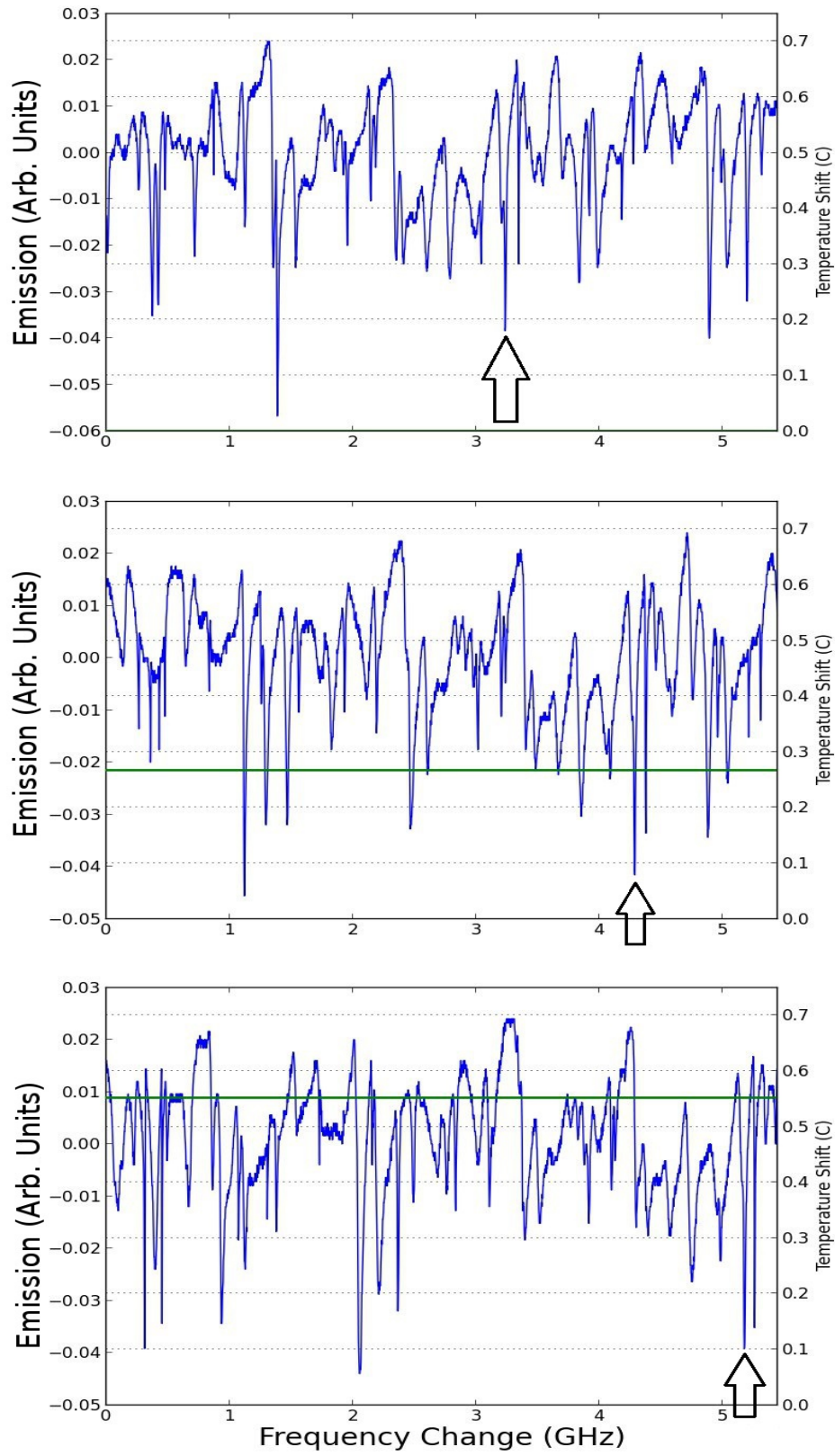


Figure 5.1: Temperature sensitivity using resonant mode frequency

the smallest temperature change that can be measured in this way:

$$\Delta T_{\text{best}} = \frac{2}{\text{SNR}} \frac{\Delta\nu}{\gamma} \quad (5.1)$$

where SNR is the signal-to-noise ratio,  $\Delta\nu$  is the mode width, and  $\gamma$  is the frequency to temperature relation from Equation (2.7). The factor of 2 comes from the response signal being twice the mode width at half-maximum. Initially, a noise level of 20 *mV* was measured, with a response signal of 20 *V*, corresponding to a scan of  $2\Delta\nu$ , yielding an SNR of 1000. The mode width at this time was 5 *MHz*. Plugging these values into Equation (5.1), along with the measured  $\gamma$  of 2.65 *GHz/K* for LiNbO<sub>3</sub>, yielded a  $\Delta T_{\text{best}}$  of 3.8  $\mu K$ . However, after the addition of a neutral density filter, the noise level was measured to be the same 20 *mV*, while the response signal amplitude was 15% of its original value, implying the noise was due to the electronic processing of the signal. Therefore, by multiplying this attenuated response signal by 6.67, the real signal amplitude could be obtained. Using this new value of  $V_{\text{res}} = 133.4$  *V*, while the same signal width and noise level was seen, yielded a new  $\Delta T_{\text{best}} \simeq 570$  *nK*. See Figure 5.2 for a typical response curve.

## 6 Conclusions and Outlooks

The ability to track changes in temperature on the level of 0.5  $\mu K$  was demonstrated. Given different crystals with higher changes to temperature and/or higher Q-factors, even greater precision could be accomplished. In this experiment, the noise level remaining at 20 *mV* after inclusion of a neutral density filter, indicated that the noise was due to electronics. By taking noise to the shot-noise level, large improvements could be made. Q-factors of  $10^{11}$  have been demonstrated, and this would also lower the smallest change able to be tracked by decreasing the mode-width. For example, a CaF<sub>2</sub> disk with  $Q \sim 10^{11}$  would increase the temperature response by a factor of 1.5 and lower the mode-width by a factor of one thousand, resulting in sensitivity down to about 40 *pK*.

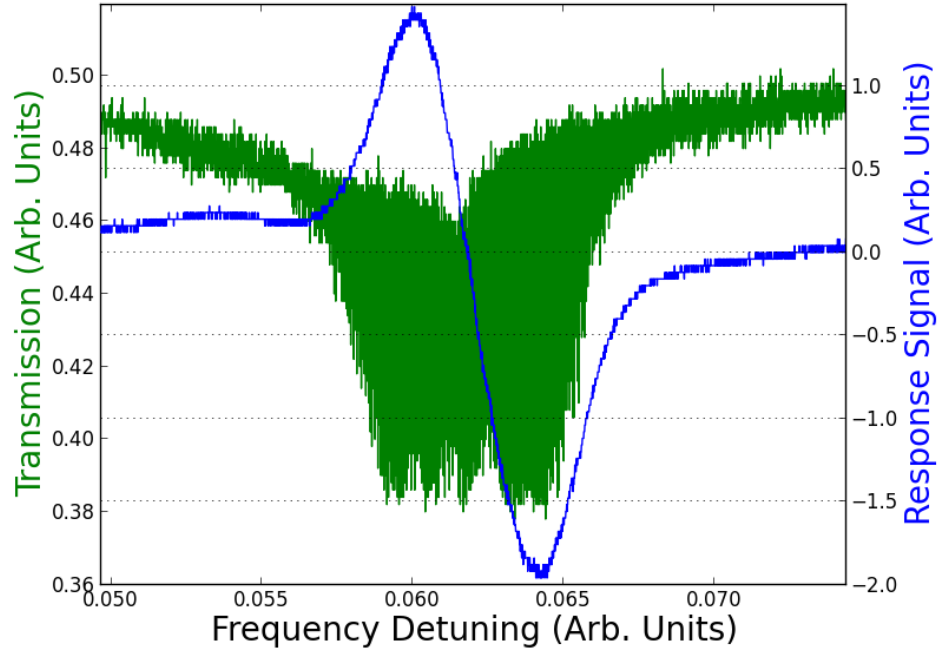


Figure 5.2: The response signal along with the mode being tracked. The noise in the mode is due to dithering the laser

Further, while temperature was the variable tracked in this experiment, any environmental factor could likewise be tracked, assuming it affects the resonator in a measurable way. These factors include pressure, electric field strength, and frequency just to name a few. Also, the small size and relative durability of these disks lend them to be used on chips or in locations that a Fabry-Perot resonator would be impractical. The relative ease of manufacture and low expense further enhances their appeal.

## 7 Acknowledgments

The author would like to thank Eugeny Mikhailov for his guiding support throughout this process, Irina Novikova for her helpful insight into problems, and Matthew Simons for his patience and entertaining conversations.



## References

- [1] Vladimir S. Ilchenko, Anatoliy A. Savchenkov, Andrey B. Matsko, and Lute Maleki. Nonlinear optics and crystalline whispering gallery mode cavities. *Phys. Rev. Lett.*, 92:043903, Jan 2004.
- [2] Liron Stern, Ilya Goykhman, Boris Desiatov, and Uriel Levy. Frequency locked micro disk resonator for real time and precise monitoring of refractive index. *Opt. Lett.*, 37:1313–1315, Apr 2012.
- [3] A.B. Matsko and V.S. Ilchenko. Optical resonators with whispering-gallery modes-part i: basics. *Selected Topics in Quantum Electronics, IEEE Journal of*, 12(1):3–14, 2006.
- [4] Anatoliy A. Savchenkov, Andrey B. Matsko, Vladimir S. Ilchenko, and Lute Maleki. Optical resonators with ten million finesse. *Opt. Express*, 15(11):6768–6773, May 2007.
- [5] N. Hodgson and H. Weber. *Optical Resonators: Fundamentals, Advanced Concepts, and Applications*. Springer Verlag, 1997.
- [6] Lute Maleki, Vladimir S. Ilchenko, Anatoliy A. Savchenkov, and Andrey B. Matsko. *Practical Applications of Microresonators in Optics and Photonics*. CRC Press, 2009.
- [7] H.J. Pain. *The physics of vibrations and waves*. John Wiley & Sons Canada, Limited, 1999.
- [8] D. N. Batchelder and R. O. Simmons. Lattice constants and thermal expansivities of silicon and of calcium fluoride between 6[degree] and 322[degree]k. *The Journal of Chemical Physics*, 41(8):2324–2329, 1964.

# Appendices

## A Polishing Technique

Polishing procedure:

- 1) Starting from a cut blank, 600 grit aluminum oxide sandpaper was used to remove material from the edge due to any cracks formed during cutting, using water as a lubricant. The lathe was set to approximately 50% of maximum speed, as indicated on the knob. Then, the sand paper was attached to a glass plate and used to bevel both the top and bottom edge until they met at a point, forming the edge. The angle of the bevel on the bottom edge was limited by the post, but a top and bottom bevel of  $\approx 45^\circ$  was used. After this step, the disk was rinsed with water and dried.
- 2) Next, the beveling was continued in the same fashion with 1000 grit aluminum oxide sandpaper, once again using water as a lubricant, removing more material, and making the edge finer. The lathe speed was still at about 50%. The time for this and the previous step depended on the amount of material to be removed. After practice, it became clear to not use too much pressure, as this created deep gouges in the disk. Once satisfied by the evenness of the surfaces after examination under a microscope, the disk was again cleaned.
- 3) The next step moved to 30  $\mu m$  particle-size lapping paper. Lathe speed was lowered to about 40%. A methanol based polishing solution was used as a lubricant and for rinsing. Continuing use of a glass plate, the bevel and surface continued to be polished/shaped. The rim itself remained untouched. After the surface again looked even under the microscope, albeit with smaller imperfections, the disk was rinsed and dried.
- 4) The next size lapping paper was 9  $\mu m$ . The methanol polishing solution was still used, and lathe speed was the same as in the previous step. This step continued as the previous

ones, taking the surface to an even finer smoothness. The rim was still not touched, and the glass plate was still used as a backer. After this step, the rim had become very sharp, and the disk was rinsed and dried.

- 5) Moving to a  $3\text{ }\mu\text{m}$  lapping paper, the methanol polishing solution was still used, but the glass plate was discontinued. Lathe speed remained as it was in the previous two steps. Attention now moved to the rim. The lapping paper was held to allow it to come into contact with a quarter to a fifth of the rim surface. It was then moved back-and-forth over the rim, beginning to round it. The rest of the disk was ignored at this point, since it played no part in the quality of the resonator. The time for this step was somewhat variable, but after two minutes of proper polishing, the rim was usually ready for the next step. To check this, the disk was first rinsed with the polishing solution, dried, then rinsed with optically clean (pure) acetone, and dried once again. The acetone removed the oily residue left by the polishing solution, allowing one to see imperfections. The surface blemishes along the rim were small now, but still visible. Any blemishes about the same size of the rim needed to be removed during this step, so if any existed, this step was repeated until they were gone.
- 6) The last lapping paper size used was  $1\text{ }\mu\text{m}$ . Lathe speed was still about 40% and the polishing solution was still used. In the same way as the previous step, the rim was polished. Once again, two minutes was a usual time. The same rinse with polishing solution, dry, rinse with acetone, and dry procedure was done before viewing it under the microscope. At this point, the disk rim had been slightly broadened by the polishing and was also somewhat curved. All the marks on the rim were invisible at this point, and if not, this step was repeated until that was the case.
- 7) The methanol polishing solution was no longer used from this point forward. In this step, a  $0.5\text{ }\mu\text{m}$  particle size diamond emulsion was used to polish. A wipe was dampened with this fluid, then cupped around the disk. Lathe speed was slightly lowered, to about 30%.

After one minute, more of the solution was added to the cup created by the wipe, creating a pool of fluid in which the disk rotated, and it was polished for another minute. During this step, the pressure used holding the wipe to the disk was somewhat firm. When too much pressure was used, the wipe would tear, and start to wrap around the disk/post, creating a potential for the disk to become disconnected from the post. However, after several polishing sessions and mishaps, a feeling for the correct pressure was found. *Note:* due to an oversight during the first time using the emulsions, acetone was not used to clean the disk between this and the next step. However, because that disk yielded the highest Q-factor yet produced in our lab ( $\sim 8 \times 10^7$ ), superstition kept that same habit for subsequent polishings. On the next polishing following this oversight,  $Q > 10^8$  was measured. It is not clear if the acetone cleaning at this stage has either no effect, limits the production of higher Q-factors, or is in some way beneficial.

- 8) Lastly, a  $0.1 \mu m$  diamond emulsion was used. The first two minutes of this step proceed in the exact same way as the previous, however after two minutes, lathe speed was lowered to 20% speed or so. As the third minute progressed, fluid was added to keep the disk in a “pool.” Further, the speed was gradually lowered throughout, eventually to the point of stopping, around the three minute mark. The disk was then cleaned with acetone, dried, and examined. At this point, any rim imperfections were too small to see with an optical microscope. If there were some remaining, then depending on their size, the procedure was picked up from one of the previous steps. Knowing exactly where to re-start came with experience after many polishing sessions.

Extra Notes:

- Both broad and narrow rim edges have been produced. Narrow rims have yielded higher Q-factors and better mode isolation, that is, less overlapping with nearby modes.

## B Coupling Plots

These plots show the coupling parameters for a  $\text{LiNbO}_3$  disk with a diamond prism.

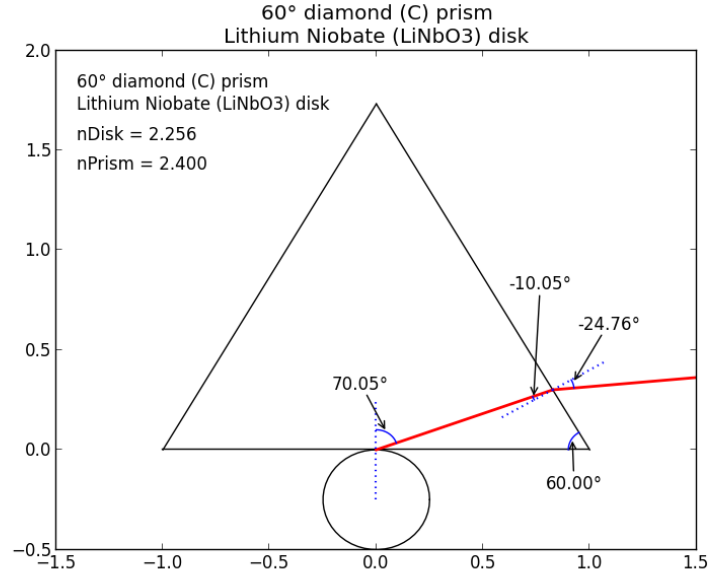


Figure B.1: Coupling Angles for Diamond Prism, Lithium Niobate Disk

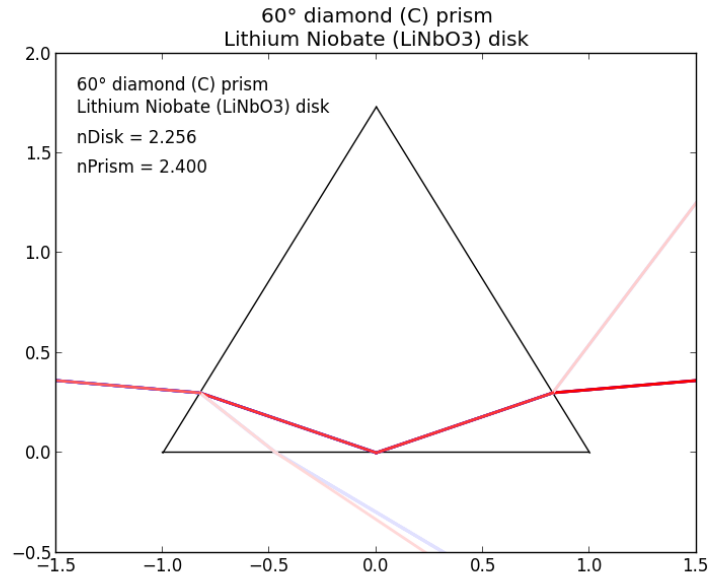


Figure B.2: Beam Trace for Diamond Prism, Lithium Niobate Disk